

UCRL-72189  
59  
31

## Soft-Sphere Equation of State\*

WILLIAM G. HOOVER, MARVIN ROSS, AND KEITH W. JOHNSON

*University of California, Lawrence Radiation Laboratory, Livermore, California 94550*

AND

DOUGLAS HENDERSON AND JOHN A. BARKER

*IBM Research Laboratory, San Jose, California 95114*

AND

BRYAN C. BROWN†

*Northwestern University, Evanston, Illinois 60201*

(Received 29 December 1969)

The pressure and entropy for soft-sphere particles interacting with an inverse twelfth-power potential are determined using the Monte Carlo method. The solid-phase entropy is calculated in two ways: by integrating the single-occupancy equation of state from the low density limit to solid densities, and by using solid-phase Monte Carlo pressures to evaluate the anharmonic corrections to the lattice-dynamics high-density limit. The two methods agree, and the entropy is used to locate the melting transition. The computed results are compared with the predictions of the virial series, lattice dynamics, perturbation theories, and cell models. For the fluid phase, perturbation theory is very accurate up to two-thirds of the freezing density. For the solid phase, a correlated cell model predicts pressures very close to the Monte Carlo results.

### I. INTRODUCTION

Fifteen years of numerical work aiming at understanding thermodynamic properties of hard spheres has led to a complete equation of state.<sup>1-4</sup> The fluid-<sup>1</sup> and solid-branch<sup>2</sup> pressures and the phase transition location<sup>3</sup> were all accurately measured by computer experiments. Although the numerical machine results do not in themselves constitute theories, it is in retrospect possible to select theories, among the many suggested, which successfully reproduce the machine results. The virial expansion works for the fluid phase,<sup>1</sup> and Fixman's theory,<sup>5</sup> supplemented by the cell-cluster calculations of the entropy constant,<sup>6</sup> describes the solid well. These are two completely different approaches; a unified hard-sphere theory analyzing both phases still appears far off.

The hard-sphere potential is inappropriate for some problems. For example, the large temperature changes in strong shock waves correspond, with a realistic potential, to large changes in effective hard-sphere diameter. The effective diameter represents an average closest-approach distance for colliding molecules. At low density this would be the separation where the pair potential is  $\sim kT$ . If two very different temperatures are involved, as in a strong shockwave, then two *different* effective diameters are needed. In such a case a soft-sphere rather than a hard-sphere potential can be used.

In this paper we use the Monte Carlo method to determine accurate thermodynamic properties for a soft-sphere potential. We then use the results to check the accuracy of approximate equation-of-state theories. Of the many soft-sphere potentials to choose from, we have picked an inverse power potential, which is the simplest kind, because a single isotherm determines all the rest, as we see in Sec. II. Among the inverse power potentials

the twelfth,

$$\phi(r) = \epsilon(\sigma/r)^{12}, \quad (1)$$

is of special interest as the high-temperature limit of the Lennard-Jones potential. The Lennard-Jones potential provides a realistic description of rare-gas interactions at pressures up to a few kilobars, and has therefore been extensively studied in computer experiments.<sup>7-10</sup>

Soft-sphere and hard-sphere properties can be correlated by perturbation theories. Rowlinson<sup>11</sup> has shown how to expand the thermodynamic properties for an inverse  $n$ th-power potential around the hard-sphere limit. The expansion parameter in this perturbation expansion is  $1/n$ . Rowlinson also noted that, to order  $1/n$ , the inverse power  $(r_0/r)^n$  and the exponential  $\exp[-n(r-r_0)/r_0]$  are identical, so that additional connections can be established between inverse-power and exponential-potential thermodynamic properties. Our Monte Carlo results show that, for  $n=12$ , Rowlinson's  $1/n$  expansion is too crude for quantitative calculations. But it is still worthwhile to consider perturbation theories, because computer-time requirements are so great for force laws more complicated than the hard sphere. However, a perturbation theory more sophisticated than Rowlinson's is needed. Barker and Henderson<sup>12</sup> have developed such a theory by combining Rowlinson's steepness expansion with Zwanzig's high-temperature expansion.<sup>13</sup> Comparing our Monte Carlo results with the Barker-Henderson predictions indicates that, except for very dense fluids, their perturbation theory is accurate. A comparison of the perturbation theory predictions with results for the full Lennard-Jones potential has recently been carried out by Levesque and Verlet.<sup>9</sup>

In our Monte Carlo work we generate exact equations of state for the fluid and the solid, and determine the boundaries of the two-phase region. In addition we

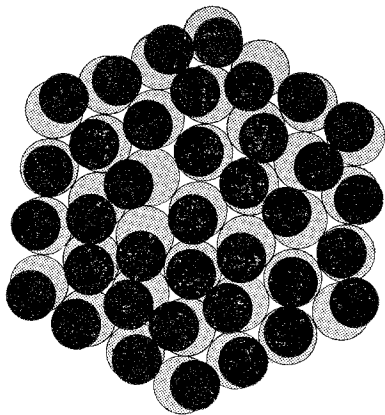


FIG. 1. A two-dimensional single-occupancy system. The particles, represented as black circles, are free to move as long as the center of each stays in its cell. The cells are the larger shaded circles. At high densities almost all collisions occur between pairs of particles and the single-occupancy thermodynamic properties are identical with those of a defect-free solid. At lower densities collisions with the cell walls can occur, and the single-occupancy system produces an artificial extension of the solid phase to low density.

study a 32-particle "single-occupancy" system over the whole density range. In a single-occupancy system, such as that shown in Fig. 1, each particle is restricted to an individual cell, the cells being arranged to impose a regular crystal structure at densities high enough for the solid to be stable. We show numerically that the thermodynamic differences between a single-occupancy solid and the more usual solid, in which the cell walls are missing, are completely negligible.

For *hard* spheres the solid-phase entropy could only be determined by integrating the single-occupancy pressure from the known low-density limit to high density.<sup>3</sup> For *soft* spheres lattice dynamics<sup>14</sup> provides an independent way to determine the solid-phase entropy, so that the soft-sphere integration provides a check on the accuracy of the Monte Carlo pressures. We also use lattice dynamics calculations to determine the number-dependence of solid-phase thermodynamic properties.

Results for the fluid-phase pressure and entropy are given in Sec. II. Along with the measured Monte Carlo pressures, we include numerical estimates for the first five virial coefficients in the density expansion of the pressure.

Results for the solid-phase pressure and entropy are given in Sec. III. The computed pressures make it possible to determine the anharmonic corrections of order  $T$  and  $T^2$  to the predictions of lattice dynamics. The single-occupancy calculation of the solid-phase entropy is compared with the lattice dynamics calculation in Sec. IV. Making use of the theoretical number-dependence of the thermodynamic properties, we establish the infinite-system melting line in Sec. V. In the final section we compare our computed results with the predictions of some perturbation theories for fluids and some cell models for solids.

## II. FLUID-PHASE PROPERTIES

In either phase, fluid or solid, the pressure  $P$  for  $N$  soft spheres in a periodic volume  $V$  and at temperature  $T$  is calculated from the virial theorem<sup>15</sup>:

$$\begin{aligned} PV/NkT &= 1 - (3NkT)^{-1} \langle \sum r\phi' \rangle \\ &= 1 + (4/NkT) \langle \sum \epsilon(\sigma/r)^{12} \rangle \\ &= (4E/NkT) - 5. \end{aligned} \quad (2)$$

The brackets indicate a canonical-ensemble average, the sums include each pair of particles in the system,  $k$  is Boltzmann's constant, and  $E = \Phi + \frac{3}{2}NkT$  is the thermodynamic internal energy. The excess entropy  $S^e$  (relative to an ideal gas at the same density and temperature) as well as the excess Helmholtz and Gibbs free energies,  $A^e$  and  $G^e$ , can be obtained by integrating the Monte Carlo pressure results:

$$\begin{aligned} \frac{S^e}{Nk} &= \frac{PV - NkT}{4NkT} - \int_0^\rho \left( \frac{PV - NkT}{NkT} \right) d \ln \rho \\ &= \frac{PV - NkT}{4NkT} - \int_0^{\epsilon/kT} (NkT)^{-1} \langle \sum \phi \rangle d \ln \frac{\epsilon}{kT} \\ &= [(PV - NkT)/4NkT] - (A^e/NkT) \\ &= 5[(PV - NkT)/4NkT] - (G^e/NkT), \end{aligned} \quad (3)$$

where  $\rho$  is the density relative to the density at which *hard* spheres of diameter  $\sigma$  would be close packed,  $\rho \equiv N\sigma^3/(\sqrt{2}V)$ . The simple scaling of temperature and density integrals in (3) and the proportionality between  $PV - NkT$  and  $E - \frac{3}{2}NkT$  in (2) are both consequences of the simple inverse power law, not general results. The scaling relations are most easily derived by writing the canonical partition function  $Z = \exp(-A/kT)$  as an integral over reduced distances,  $\mathbf{s}_i \equiv (N/V)^{1/3} \mathbf{r}_i$ :

$$Z = e^{-A/kT} = \left( \frac{(V/N\Lambda^3)^N}{N!} \right) \int \exp \left[ - \left( \frac{4\rho^4\epsilon}{kT} \right) \sum s_{ij}^{-12} \right] d\mathbf{s}^{3N}, \quad (4)$$

where  $\Lambda$  is the thermal de Broglie wavelength  $h/(2\pi mkT)^{1/2}$ . Because the integrand is a function of  $\rho^4\epsilon/kT$  only and the integration limits are independent of  $V$  and  $T$ , the *excess* thermodynamic properties (with respect to an ideal gas in  $V$  at  $T$ ) are functions of  $\rho^4\epsilon/kT$  only. For this reason a single isotherm or isochore determines the entire equation of state. For simplicity we sometimes speak of "low density" or "high density" in this paper, having in mind a fixed temperature. The same regions, from a fixed-volume viewpoint, could equally well be described as "high temperature" or "low temperature."

For numerical calculation of excess entropy from the Monte Carlo pressures, it is convenient to consider excess properties with respect to an ideal gas in the constant external field  $\Phi_0$ , where  $\Phi_0$  is the energy of a static lattice (depending on  $V$  but not  $T$ ). By subtracting the dominant static-lattice contribution to the

pressure, the accuracy of the integration determining  $S^e$  is improved. Compare Figs. 2 and 3, which show the 32-particle single-occupancy equation-of-state data plotted in two ways: In Fig. 2 the Helmholtz free energy relative to an ideal gas is determined by integrating the steeply rising ( $\sim\rho^4$ ) integrand. In the process of calculating  $S^e$  from (3), the static-lattice contribution has to be subtracted from the integral. In Fig. 3 the static-lattice contribution is left out before plotting the data ( $P^*$  is  $P - P_{\text{static}} - P_{\text{ideal}}$ ) and the change in the entropy-determining integrand is reduced by an order of magnitude. As the figures show, entropy changes can be calculated by either temperature or density integrations.

The fluid-phase Monte Carlo pressure calculations for 32 and 500 soft spheres are summarized in Table I. No number-dependent lattice corrections or center-of-mass corrections have been made in the tabulated data. Lattice corrections add in the effect of particles outside the periodic Monte Carlo volume. For 32 particles this effect would increase our "nearest-image" value for the compressibility factor  $PV/NkT$  by  $0.136\rho^4\epsilon/kT$ ; the correction for 500 particles is negligible for the densities investigated. The center-of-mass correction is more important. Because there is no restoring force opposing motion of the system as a whole, three degrees of freedom make ideal-gas contributions to the thermal (nonstatic) part of the pressure. Because center-of-mass motion makes no contribution in the thermodynamic limit, its contribution should be removed when estimating infinite-system properties. To make this correction the excess compressibility

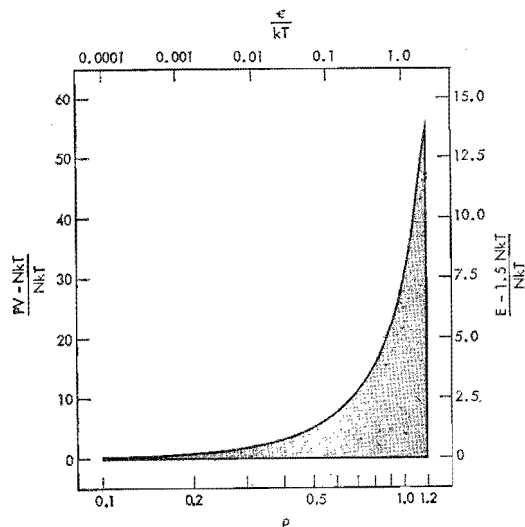


FIG. 2. Equation of state for 32 single-occupancy soft spheres, plotted with the integration of Eq. (3) indicated by shading. The shaded area is  $[A^e(\rho=1.2) - A^e(\rho=0.1)]/NkT$  for the isotherm  $\epsilon/kT=1$ . The proportionality of the pressure and energy scales and the logarithmic temperature and density scales is a consequence of the inverse twelfth-power potential used. The temperature scale corresponds to the case  $\rho=1$ . At high density the integrand is proportional to  $\rho^4$ .

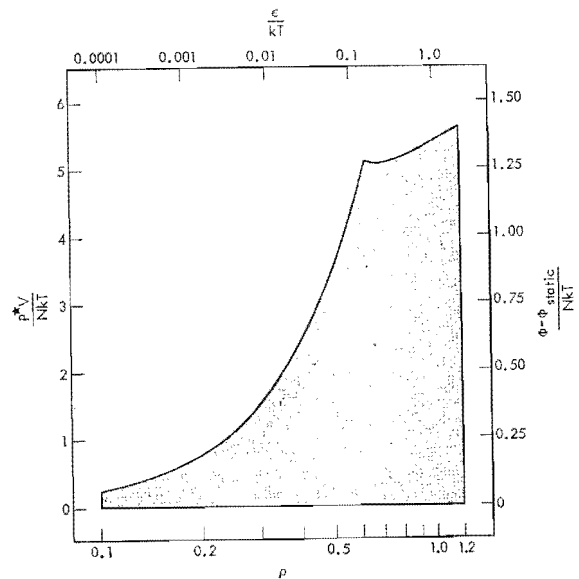


FIG. 3. Equation of state for 32 single-occupancy soft spheres, plotted with the integration of Eq. (12) indicated by shading. The temperature scale applies to the case  $\rho=1$ ; the density scale to  $\epsilon/kT=1$ . The static-lattice and ideal-gas contributions to the pressure and energy are subtracted to increase the accuracy of this calculation over that shown in Fig. 2. The shaded area is  $[TS(0.1) - TS(1.2) - \frac{1}{2}VP^*(0.1) + \frac{1}{2}VP^*(1.2)]/NkT$ . The sharp break in the equation of state occurs when the particles first contact the cell walls. In Fig. 2 the break is disguised by the static-lattice contribution to the pressure.

factor,  $P^*V/NkT$ , should be multiplied by a factor of  $N/(N-1)$ , 1.0020 for 500 particles. This correction is never larger than 0.02 for 500 particles.

For hard spheres the virial series, augmented by the Padé method, predicts the entire fluid equation of state.<sup>1</sup> To test the usefulness of the virial series for soft spheres we calculated the first five terms in the density expansion of  $PV/NkT$  using the methods outlined by Barker, Leonard, and Pompe.<sup>16</sup> The resulting equation of state is

$$\begin{aligned} PV/NkT &= 1 + x + 0.5755x^2 + 0.2087x^3 + 0.0487x^4 + \dots, \\ x &= \frac{2}{3}\pi\sigma^3(N/V)(\epsilon/kT)^{1/4}\Gamma(\frac{3}{2}) \\ &= 3.62959\rho(\epsilon/kT)^{1/4}. \end{aligned} \quad (5)$$

Up to about half the freezing density [found to be  $\rho=0.813(kT/\epsilon)^{1/4}$  in Sec. V] the truncated five-term series agrees with the machine results. The maximum deviation is about 1% in  $PV/NkT$ . As the density is increased the error grows, reaching about 10% at freezing. By analogy with our earlier work with hard spheres<sup>1</sup> and Gaussian molecules<sup>17</sup> we expected that the Padé approximant reproducing (5),

$$\begin{aligned} PV/NkT &= (1 + 0.4180x + 0.1198x^2)/(1 - 0.5820x + 0.1263x^2), \end{aligned} \quad (6)$$

would be an improvement over the truncated series.

TABLE I. Fluid-phase thermodynamic properties for inverse twelfth-power systems. In addition to the compressibility factor, determined from 0.3 million Monte Carlo configurations for  $\rho(\epsilon/kT)^{1/4} < 0.70$  and up to 2.5 million configurations for higher densities, the entropy relative to an ideal gas at the same temperature and density is tabulated. Because the ideal-gas standard corresponds to the partition function  $Z_{ideal} = (Ve/N\Lambda^3)^N$ , the finite-system entropy lies below the ideal gas entropy even at zero density. The Helmholtz and Gibbs free energies can be obtained from the pressure and entropy data by using Eq. (3) of the text. The pressure data are expected to be accurate within 0.05 or better in  $PV/NkT$ . The entropy data are accurate within 0.02Nk. The quoted infinite-system results are smoothed estimates derived from the 500-particle data by taking the center-of-mass and zero-density entropy corrections into account.

$\rho(\epsilon/kT)^{1/4}$	$(PV/NkT)_{32}$	$(S^e/Nk)_{32}$	$(PV/NkT)_{500}$	$(S^e/Nk)_{500}$	$(PV/NkT)_{\infty}$	$(S^e/Nk)_{\infty}$
0.00	1.000	-0.083	1.000	-0.008	1.000	-0.000
0.10	1.439	-0.367	1.447	-0.299	1.448	-0.291
0.20	2.108	-0.695	2.119	-0.633	2.121	-0.626
0.30	3.081	-1.073	3.096	-1.014	3.101	-1.008
0.40	4.553	-1.495	4.548	-1.440	4.557	-1.434
0.50	6.604	-1.970	6.634	-1.923	6.641	-1.918
0.60	9.451	-2.524	9.560	-2.470	9.460	-2.465
0.65			11.267	-2.769	11.357	-2.764
0.70	13.182	-3.155	13.492	-3.084	13.469	-3.079
0.74			15.351	-3.348	15.395	-3.343
0.77			16.987	-3.548	17.006	-3.543
0.80			18.763	-3.754	18.762	-3.749

The approximant (6) is, however, vastly inferior to the truncated series, predicting a pressure too low by a factor of 2 at freezing; we have checked that this conclusion is not affected by the uncertainty in our calculated virial coefficients. This shows the value of considering more than one or two special cases before assuming the validity of simple general rules!

The entropy data given in Table I were calculated by numerical integration, carried out along the lines of Fig. 3. The table shows that the number dependence of the entropy is insensitive to density, the difference between the 32-particle and 500-particle results staying roughly constant. Most of the difference is accounted for by the low-density limit,<sup>18</sup>

$$\exp\left(\frac{S^e}{k}\right) = \frac{(N/e)^N}{N!} \cong (2\pi N)^{-1/2}.$$

### III. SOLID-PHASE PROPERTIES

The solid-phase calculations proceed just as in the fluid case, except that the density is so high that the initial face-centered arrangement persists throughout the calculation. As the analog of the low-density ideal-gas limit for the fluid, we have the high-density lattice-dynamics limit for a solid. For  $\rho(\epsilon/kT)^{1/4} \gg 1$  the harmonic approximation of lattice dynamics becomes exact. If the potential energy  $\Phi = \sum \phi$  is expanded in powers of the displacements of the particles relative to the center-of-mass displacement, and if the resulting expression is truncated after quadratic terms, the quadratic form can be diagonalized and the partition function integrated to give  $Z_{\text{harmonic}}$  in terms of the lattice vibration frequencies,  $\{\nu_j\}$ :

$$Z_{\text{harmonic}} = \exp\left(-\frac{\Phi_0}{kT}\right) \frac{V}{N} \frac{N^{3/2}}{\Lambda^3} \prod_{j=1}^{3N-3} \frac{kT}{h\nu_j}, \quad (7)$$

where the center-of-mass contribution is<sup>19</sup>

$$(V/N) (\Lambda^{7/2}/\Lambda^3).$$

At densities too low for (7) to hold, a perturbation expansion can be used to extend its usefulness:

$$Z = Z_{\text{harmonic}} \exp[-NC_1(kT/\rho^4\epsilon) - NC_2(kT/\rho^4\epsilon)^2 - \dots]. \quad (8)$$

It should be emphasized that  $Z_{\text{harmonic}}$ ,  $C_1$ ,  $C_2$ ,  $\dots$  depend upon the number of particles.  $Z_{\text{harmonic}}$  depends also on  $\rho$  and  $T$ .  $\Phi_0$  is proportional to  $\rho^4$  and the vibration frequencies follow a Grüneisen description, all being proportional to  $\rho^{7/3}$ . The number dependence of  $Z_{\text{harmonic}}$  has been established empirically. It was found,<sup>20</sup> for nearest-neighbor Hooke's Law crystals,

TABLE II. Entropy constants for periodic face-centered crystals of soft spheres interacting with an inverse twelfth-power potential. The constants  $C(N)$  are  $1/N$  times the sum, over  $3N-3$  nonzero oscillation frequencies,  $\{\nu_j\}$ , of  $\ln(\nu_{\text{Einstein}}/\nu_j)$ , where  $\nu_{\text{Einstein}}$  is the Einstein frequency.

$N$	$C(N)$	$C(N) + \ln N/N$	$\nu_{\text{Einstein}} \sigma (m/\epsilon)^{1/2} \rho^{-7/3}$
4	-0.22108	0.12550	1.8286
32	+0.20970	0.31801	3.6615
108	0.28850	0.33185	3.6661
256	0.31464	0.33630	3.6661
500	0.32553	0.33796	3.6661
864	0.33088	0.33870	3.6661
1372	0.33381	0.33908	3.6661
2048	0.33557	0.33929	3.6661
2916	0.33668	0.33942	3.6661
4000	0.33743	0.33950	3.6661
$\infty$	0.33972	0.33972	3.6661

TABLE III. Solid-phase thermodynamic properties for inverse twelfth-power systems. The 32-particle results are for a single-occupancy system. The 500-particle results were calculated without the single-occupancy constraint. The entropy data were obtained by fitting the Monte Carlo pressure to Eq. (8) of the text, using the entropy constants from Table II. The infinite-system estimates use the infinite-system entropy constant  $C$  from Table II and the  $C_1$  and  $C_2$  estimated for 500 particles,  $+0.0875$  and  $-0.009$ , respectively.

$\rho(\epsilon/kT)^{1/4}$	$(PV/NkT)_{32}$	$(S^e/Nk)_{32}$	$(PV/NkT)_{500}$	$(S^e/Nk)_{500}$	$(PV/NkT)_\infty$	$(S^e/Nk)_\infty$
0.74			$\sim 14.14$	$-3.867$	13.91	$-3.945$
0.80	16.05	$-4.390$	16.55	$-4.371$	16.51	$-4.395$
0.90	22.11	$-4.980$	22.51	$-5.042$	22.55	$-5.040$
1.00	30.55	$-5.507$	30.99	$-5.630$	30.99	$-5.616$
1.20	56.65	$-6.463$	57.15	$-6.637$	57.16	$-6.640$

that

$$N^{-1} \ln \prod_{j=1}^{3N-3} \left( \frac{\nu_j^{\text{Einstein}}}{\nu_j} \right) \equiv C(N) \\ \doteq C - (\ln N/N) + O(N^{-1}). \quad (9)$$

The Einstein frequency, also proportional to  $\rho^{2/3}$ , is the frequency at which a single particle oscillates if all the other particles are held fixed in a perfect-lattice arrangement. We found that (9) also holds for soft-sphere crystals. By computing the oscillation frequencies for various sized crystals<sup>14</sup> (using the same nearest-image convention used in the Monte Carlo work), we obtained the large-system limit  $C$  and verified the  $\ln N/N$  dependence of  $C(N)$ . Results are given in Table II.

The anharmonic corrections in (8),  $C_1$  and  $C_2$ , must both be used to fit the solid-phase Monte Carlo data up to the melting point. Theoretical calculations of anharmonic terms<sup>21</sup> generally aim to find  $C_1$ . Terms up to sixth order in the particle displacements contribute to  $C_2$ . The computer results for 500 soft spheres in the solid phase are given in Table III. The data can be fitted within their statistical accuracy by the approximations  $C_1 = 7/80$ ,  $C_2 = -9/1000$ . The 32-particle data in the table are consistent with a larger value for  $C_1$ ,  $23/200$ , and about the same value for  $C_2$ ,  $-19/2000$ .

Without definite knowledge of the dependence of  $C_1$  and  $C_2$  on  $N$ , we have used the 500-particle estimates to calculate the thermodynamic properties for infinite crystals listed in the table. Also listed in the table are the entropies calculated from (8) using the Monte-Carlo estimates of  $C_1$  and  $C_2$  for 32 and 500 soft spheres.

## IV. TEST OF THE SINGLE-OCCUPANCY MODEL

The single-occupancy model, which we here use for soft spheres, was first used to determine the solid-phase hard-sphere entropy.<sup>3</sup> It is the only numerical way to determine the hard-sphere entropy, because the pressure fluctuations near the melting transition make direct integration of the pressure inaccurate. For soft spheres, the single-occupancy model is not the only way to find the solid-phase entropy; the lattice-dynamics method we used in Sec. III is an alternative. Thus, by comparing our soft-sphere entropy results from Sec. III with calculated entropies from the soft-sphere single-oc-

cupancy model, we check the accuracy of the single-occupancy approach. This is an indirect test of the validity of the previous hard-sphere<sup>3</sup> and Lennard-Jones potential<sup>7</sup> calculations.<sup>22</sup>

By enforcing perfect crystalline order the model ignores the dislocations, grain boundaries, and vacancies that are present in real crystals. The most important of these defects, vacancies, can be treated theoretically;<sup>23,24</sup> for soft spheres it is found that the fraction of vacancies at melting is of order  $\exp(-PV/NkT)$ .<sup>25</sup> This small defect population has a negligible effect on solid-phase bulk thermodynamic properties, justifying the use of the artificially structured single-occupancy restriction.

Previous calculations<sup>3,7</sup> used dodecahedral Wigner-Seitz cells to confine the particles. To simplify the geometry we here use spherical cells. The cell diameter used is equal to the nearest-neighbor spacing in a perfect face-centered cubic crystal. Our results show that in the density region in which the solid is thermodynamically stable it makes no difference whether the cells are dodecahedra or spheres. At low density, where the single-occupancy method gives a metastable extension of the solid phase, results do depend on cell geometry. The spherical cells are smaller, by a factor of  $3\sqrt{2}/\pi \doteq e^{0.3005}$ , and this different low-density limit must be taken into account in entropy calculations.

At densities up to about  $0.1(kT/\epsilon)^{1/4}$  a Mayer  $f$ -function expansion of the partition function gives the thermodynamic properties of the single-occupancy system in terms of a two-particle integral:

$$Z_{so} \doteq \left( \frac{V_{\text{cell}}}{\Lambda^3} \right)^N \exp \left[ \left( \frac{1}{2} \frac{Nz}{V_{\text{cell}}^2} \right) \int_{\Delta} \int_{\Delta} (e^{-\phi/kT} - 1) d\mathbf{r}_1 d\mathbf{r}_2 \right]. \quad (10)$$

Particles 1 and 2 occupy adjacent cells in the integration, and  $z$  is the coordination number, 12 for a face-centered crystal. For hard spheres confined to spherical cells the integral can be worked out analytically:

$$\int_{\Delta} \int_{\Delta} (e^{-\phi/kT} - 1) d\mathbf{r}_1 d\mathbf{r}_2 = - \frac{\pi^2 \sigma^6 (42\rho^{-1/3} - 35 + 6\rho^{1/3})}{1260}, \quad (11)$$

where  $\sigma$  is the sphere diameter; this form serves as a

TABLE IV. Single-occupancy thermodynamic properties for 32 soft spheres with periodic boundaries. Each sphere is confined by a spherical cell, with diameter equal to the nearest-neighbor spacing. In addition to the compressibility factor, entropy, and Helmholtz free energy (with respect to an ideal gas at the same density and temperature), the excess properties with respect to an ideal gas in a mean field equal to the static-lattice energy,  $\Phi_0$ , are also given, indicated by stars. Use of these functions reduces rounding errors in numerical integrations. Because entropy is independent of an imposed constant field, the relation  $(S^e/Nk) = (S^e/Nk)^*$  holds.

$\rho(\epsilon/kT)^{1/4}$	$(PV/NkT)$	$(PV/NkT)^*$	$(S^e/Nk)$	$(A^e/NkT)$	$(A^e/NkT)^*$
0.00	1.000	0.000	-1.300	1.300	1.300
0.10	1.245	0.243	-1.395	1.457	1.456
0.20	1.806	0.767	-1.578	1.780	1.770
0.30	2.730	1.534	-1.835	2.268	2.219
0.40	4.116	2.498	-2.164	2.943	2.789
0.50	6.129	3.621	-2.560	3.842	3.465
0.55	7.407	4.199	-2.787	4.389	3.837
0.60	8.880	4.753	-3.082	5.008	4.226
0.65	10.393	5.086	-3.353	5.701	4.624
0.70	11.861	5.068	-3.733	6.448	5.000
0.80	16.054	5.171	-4.390	8.154	5.683
0.90	22.107	5.277	-4.980	10.257	6.299
1.00	30.546	5.418	-5.507	12.894	6.862
1.20	56.655	5.623	-6.463	20.377	7.869

guide in extrapolating the low-density single-occupancy results for soft spheres to zero density.<sup>26</sup>

Comparing the low-density soft-sphere entropy with the lattice-dynamics entropy from Sec. III gives the theoretical entropy difference between the low- and high-density limits. At the same time, by measuring  $-(\partial A_{so}/\partial V)_T \equiv P_{so}$  as a function of density, the entropy difference can also be determined numerically by integration, as shown in Fig. 3:

$$\frac{S^e(\rho) - S^e(0)}{Nk} = \frac{P^*V}{4NkT} - \int_0^\rho \frac{P^*V}{NkT} d \ln \rho, \quad (12)$$

where  $P^* \equiv P - P_{static} - P_{ideal}$ . At the highest density studied,  $\rho = 1.2(kT/\epsilon)^{1/4}$ , the 32-particle excess entropy (with respect to an ideal gas at the same density and temperature) was found from (12) to be  $-6.46Nk$ . The Monte Carlo pressures used in the integration are listed in Table IV. If we instead fit the high-density 32-particle pressure data to (8) with  $C_1 = 23/200$ ,  $C_2 = -19/2000$ , and the entropy constant  $C(32) = 0.210$  from Table II, the calculated excess entropy is  $-6.45Nk$ . This agreement indirectly confirms the validity of the hard-sphere calculations, and at the same time shows that any systematic errors in the Monte Carlo pressures must be less than 0.01 in  $PV/NkT$ .

We also wanted clear cut evidence that the effect of the cell walls in the single-occupancy system is negligible at all solid densities. Because the cell walls must have maximum effect at low densities, near melting, we have studied the magnitude of this effect by making a pair of "solid-phase" calculations at a density so low,  $0.8(kT/\epsilon)^{1/4}$ , that the fluid is actually the thermodynamically stable phase. We carried out two 500-particle runs of 0.3 million moves each, identical except for the single-occupancy restriction; one run

included the cell walls; the other did not. For the full length of the 0.3 million moves, both runs remained exactly identical, showing that never did any particle approach a cell boundary. This shows that the 500-particle solid-phase data in Table III, generated without cell walls, would have been unchanged by the single-occupancy restriction. Because center-of-mass drift must eventually cause particles to near the cell walls, we continued the single-occupancy problem for an additional 0.8 million moves, finding a total of 14 cell-wall collisions. This low frequency of cell-wall collisions, of order  $10^{-5}$  at densities for which the fluid is stable, indicates that the single-occupancy restriction introduces only an insignificant error, of roughly the same order as that due to the neglect of vacancies.

## V. MELTING TRANSITION

Knowing the thermodynamic properties of both phases makes it possible to locate the melting line. The simplest way is to find the density at which the Helmholtz free energies of the metastable fluid and the single-occupancy solid are equal, and then to use the equal-area rule<sup>27</sup> to find the densities at which the two stable phases coexist at equal pressure, temperature, and Gibbs free energy per particle. The most time-consuming part of the numerical work turned out to be determining the equation of state for the dense fluid. By analogy with hard spheres we expected that, in the density region where the fluid phase is stable, a 500-particle soft-sphere system would melt easily from the initial face-centered arrangement. In practice the soft-sphere system was found to be much more sluggish than the hard-sphere system.

At  $\rho(\epsilon/kT)^{1/4} = 0.70$  the soft-sphere compressibility factor rose from the static-lattice value, 5.83, to about 12.5 after 0.075 million moves, to 13 after 0.125 million

moves, and finally began to oscillate around the equilibrium value, 13.5, after 0.2 million moves. The run was extended to a million configurations to confirm this value.

At the next higher density,  $\rho(\epsilon/kT)^{1/4}=0.74$ , still well within the stable fluid phase, the compressibility factor increased from the static value, 7.28, to about 14, nearly the harmonic lattice-dynamics value, after 0.06 million moves. Then, over the next 0.4 million moves, the pressure slowly rose at a constant rate to a plateau at 15.35, where an additional million configurations were generated.

Because this evidence indicated fantastically long times to melt and reach equilibrium at higher densities, the fluid data at 0.77 and 0.80 were generated in a different way. We took the final  $\rho(\epsilon/kT)^{1/4}=0.74$  configuration and scaled the interparticle distances to correspond to a higher density,  $\rho(\epsilon/kT)^{1/4}=0.77$ , after which the problem was run for 1.5 million moves. We compared this run with a second  $\rho(\epsilon/kT)^{1/4}=0.77$  calculation starting with *random particle coordinates*. After 1.5 million moves the two estimates agreed; thus either method, sudden compression or random start, is suitable at this density. At the highest density investigated in the fluid phase,  $\rho(\epsilon/kT)^{1/4}=0.80$ , we ran a random-start problem for 2.5 million moves. In both random-start problems the initial 0.2 million moves were discarded in computing average pressures.

The fluid equation of state that finally resulted is shown in Fig. 4 for the isotherm  $\epsilon=kT$ . On that isotherm the infinite-system fluid density at freezing is  $0.813\pm 0.006$ . The density of the coexisting solid is  $0.844\pm 0.006$ . The transition pressure is  $PV_0/NkT=15.95\pm 0.3$ , and the entropy of fusion is  $[0.89\pm 0.02]Nk$ , about 25% less than the hard-sphere value.<sup>3</sup>

This fusion entropy corresponds to Ross and Alder's estimate for argon<sup>28</sup> at  $\sim 1000^\circ\text{K}$ . Their melting rule, on the other hand, which states that the fluid side of the transition should be identified with the highest density at which the initial solid configuration melts, probably underestimates the transition density by a few percent.

Because our results correspond to the high-temperature limit of the Lennard-Jones potential,

$$\phi_{\text{LJ}} = \epsilon \left[ (r_0/r)^{12} - 2(r_0/r)^6 \right], \quad (13)$$

we compared our pressures with Wood's isotherm at  $kT/\epsilon=100$ ,<sup>39</sup> and found that, even at that high temperature, the attractive term's effect is to lower the pressure on the order of 10%. For temperatures so high that the attractive contributions can be ignored our results predict

$$\begin{aligned} (PV_0/N\epsilon)_{\text{melt}} &= 15.95(kT/\epsilon)^{5/4}, \\ \rho_{\text{fluid}} &= 0.813(kT/\epsilon)^{1/4}, \\ \rho_{\text{solid}} &= 0.844(kT/\epsilon)^{1/4}. \end{aligned} \quad (14)$$

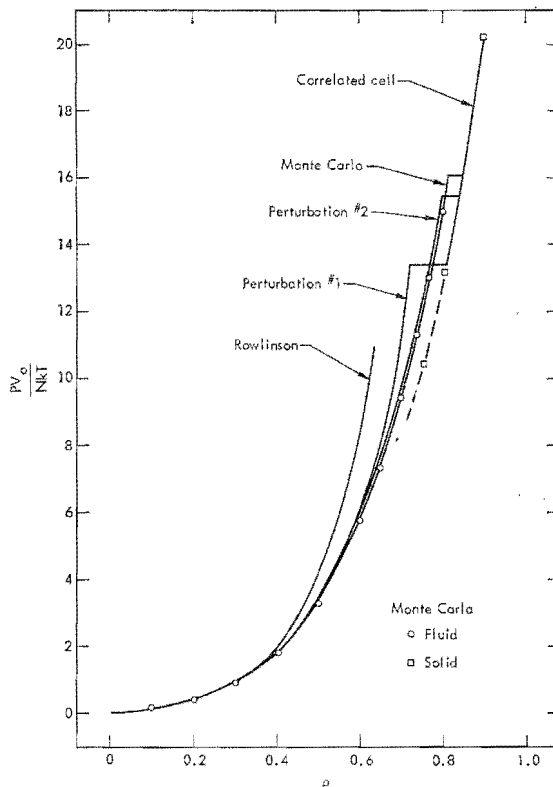


FIG. 4. Comparison of Monte Carlo data for 500 soft spheres with four approximate equations of state.  $V_0 \equiv N\sigma^3/\sqrt{2}$ . The curves drawn are the isotherms,  $\epsilon/kT=1$ . The curve labeled Rowlinson shows the result of keeping first-order terms in a  $1/n$  expansion of the partition function for inverse  $n$ th-power potentials. The Perturbation #1 curve is calculated from the Barker-Henderson theory, assuming a break point  $\mu$  between the steep and weak parts of the potential such that  $\phi(r=\mu)=kT$ . The Perturbation #2 curve uses a break point  $\mu$  chosen to minimize the variation of  $A$  with  $\mu$  (see Fig. 6 for the  $\mu$  which results). The phase-transition predictions of the perturbation theories are based on the use of the usual cell model (with spherical smearing) for the solid phase. The correlated cell model, in which three particles simultaneously move, as shown in Fig. 7, predicts pressures fitting the solid branch of the Monte Carlo equation of state within the accuracy of the latter. The location of the Monte Carlo solid-fluid tieline corresponds to equal values of the Gibbs free energy per particle in both phases.

## VI. APPROXIMATE THEORIES

In view of the poor convergence found for the five-term virial series in Sec. II, the alternative perturbation-theory approaches to the fluid equation of state are well worth pursuing. Computer time can be saved by taking advantage of *known* hard-sphere results, using these as the basis of perturbation calculations. In practice, perturbation calculations are seldom extended beyond one or two terms in the expansion parameters, so that a wise choice of these parameters is essential.

Rowlinson<sup>11</sup> expanded the partition function for the potential  $\epsilon(\sigma/r)^n$  around the hard-sphere  $\epsilon(\sigma/r)^\infty$  limit, using  $1/n$  as the expansion parameter. For our soft-sphere case his theory, truncated to first order in  $1/n$ , predicts for the isotherm  $\epsilon/kT=1$

$$(PV)_{12} = (PV)_{\infty} \quad \text{for} \quad \rho_{12} = (12/11)^3 \rho_{\infty}. \quad (15)$$

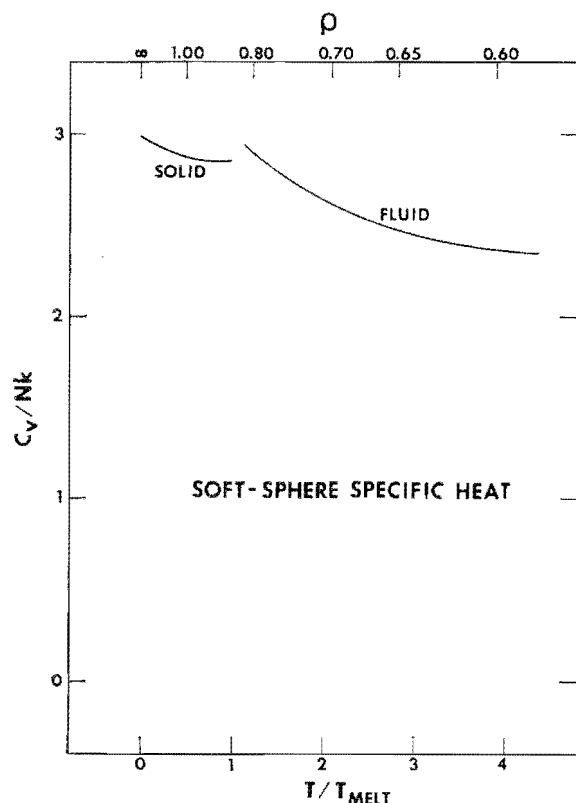


FIG. 5. Specific heat for soft spheres. The solid-phase data were derived from the approximate partition function (8) and have an uncertainty of about  $0.1Nk$  near melting. The fluid data were derived from (17), which required estimating the fluid compressibility numerically. The fluid data also have an uncertainty of  $0.1Nk$  near freezing. The temperature scale at the base of the graph corresponds to heating the solid at constant volume, illustrating Grover's rule that specific heat decreases linearly with temperature,  $C_v/Nk = 3[1 - \alpha\tau]$ , where  $\alpha = 0.05$  and  $\tau = T/T_{\text{melt}}$ . The density scale at the top of the graph corresponds to the isotherm  $\epsilon/kT = 1$ .

This predicted isotherm is shown in Fig. 4 for comparison with the Monte Carlo results. At densities where the predicted pressure is accurate an estimate from one or two virial coefficients would do just as well.

Another way to estimate the closeness of the soft-sphere system to the hard-sphere limit is to examine the specific heat.  $C_v/Nk$  is 1.5 at all densities for hard spheres, and is higher for soft spheres, reaching 3.0 at high density. In the solid phase the specific heat can be estimated from (8):

$$(C_v/Nk)_{\text{solid}} \approx 3 - 2C_1(kT/\rho^4\epsilon) - 6C_2(kT/\rho^4\epsilon)^2. \quad (16)$$

For the fluid the equivalence of density and temperature differentiations following from (4) leads to the relation

$$\left(\frac{C_v}{Nk}\right)_{\text{fluid}} = \frac{3}{2} + \frac{P^*V}{4NkT} - \frac{1}{16} \left( \frac{\partial(P^*V/NkT)}{\partial \ln \rho} \right)_T. \quad (17)$$

The specific heats from (16) and (17) appear in Fig. 5 and can be seen to lie well above the hard-sphere limit. Both the solid and the fluid specific heats show a tendency to increase near the melting transition. De-

spite these increases the data strikingly obey Grover's rule that  $C_v/Nk \approx 3(1 - \alpha\tau)$ , where  $\alpha = 0.05 \pm 0.01$  and  $\tau$  is the temperature divided by the melting temperature.<sup>30</sup> This empirical rule, established experimentally for several metals, holds for soft spheres as well. It is well worth emphasizing that the uncertainty in the computer-generated specific heats is quite large, of order  $0.1Nk$ .

Zwanzig<sup>13</sup> has considered a high-temperature perturbation theory based on the expansion

$$\frac{\int \exp[-(E + \delta E)/kT] d\Omega}{\int \exp[-E/kT] d\Omega} = 1 - \left\langle \frac{\delta E}{kT} \right\rangle + \frac{1}{2} \left\langle \left( \frac{\delta E}{kT} \right)^2 \right\rangle - \dots. \quad (18)$$

This approach, by itself, is not particularly useful for potentials lacking a hard core. Barker and Henderson<sup>12</sup> have recently combined the best features of Rowlinson's and Zwanzig's attacks by considering a two-parameter expansion. The potential is first divided up into a *steep* part ( $r < \mu$ ) and a *weak* part ( $r > \mu$ ). In the steep region the potential is expanded around a hard-sphere potential of diameter  $d$ :

$$d \equiv - \int_0^\mu (e^{-\phi/kT} - 1) dr. \quad (19)$$

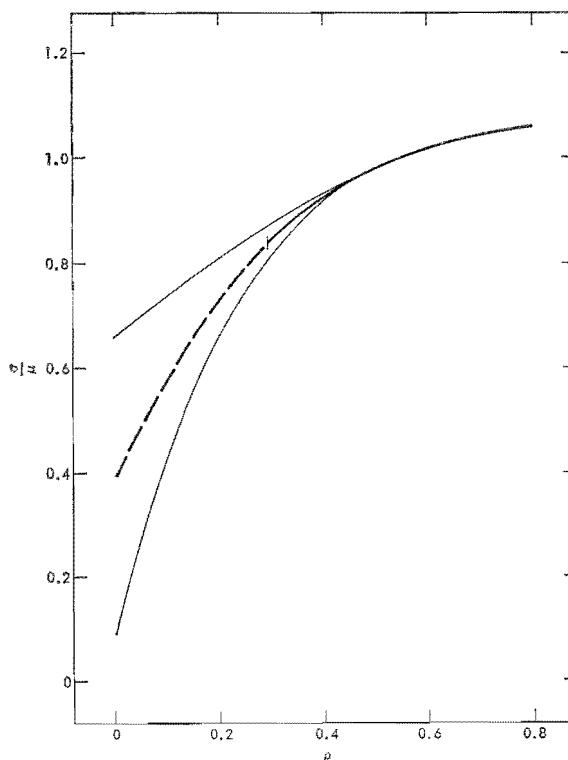


FIG. 6. Variation of the perturbation-theory break point  $\mu$  with density on the isotherm  $\epsilon/kT = 1$ . The choice of  $\mu$  at densities below 0.3, where the minimum in  $A$  disappears, is somewhat ambiguous. At these lower densities any choice  $\mu$  within the range indicated by the full curves results in the same value for the compressibility factor, within 0.01 at  $\rho = 0.3$ , and less at lower densities.

TABLE V. Compressibility factors and Helmholtz free energies for the fluid are compared with the predictions of perturbation theory. In Perturbation #1, the break point of the potential is taken at  $\phi = kT$ . In Perturbation #2 the break point is chosen to minimize the variation of Helmholtz free energy with respect to break point. The results all refer to the isotherm,  $\epsilon/kT = 1$ .

$\rho$	$(PV/NkT)_\infty$	$(PV/NkT)_1$	$(PV/NkT)_2$	$(A^\circ/NkT)_\infty$	$(A^\circ/NkT)_1$	$(A^\circ/NkT)_2$
0.10	1.45	1.47	1.36	0.40	0.42	0.39
0.20	2.12	2.15	2.11	0.91	0.94	0.89
0.30	3.10	3.16	3.18	1.53	1.58	1.54
0.40	4.56	4.65	4.72	2.32	2.40	2.37
0.50	6.64	6.89	6.93	3.33	3.43	3.43
0.60	9.46	10.31	9.98	4.60	4.79	4.77
0.65	11.36	12.70	11.88	5.35	5.62	5.57
0.70	13.47	15.73	14.13	6.20	6.60	6.46
0.75	15.91	19.63	16.61	7.14	7.74	7.45
0.80	18.76	24.74	19.57	8.19	9.10	8.55

This choice of  $d$  eliminates Helmholtz free energy contributions which would be linear in the steepness parameter. In the weak region the potential is multiplied by a strength parameter analogous to  $1/kT$ . It is important to select the break point  $\mu$  dividing the steep and weak regions with care. If the division is made at infinity and only first-order terms in  $1/n$  are kept, Rowlinson's theory results. If the division is made at  $\sigma$ , which seems a natural first guess, then the results, truncated after first-order terms in the steepness and strength parameters, are much better (see the curve marked Perturbation #1 in Fig. 4). It seems most logical however, to choose  $\mu$  in such a way that the partition function is insensitive to the choice—this corresponds to minimizing the Helmholtz free energy with respect to  $\mu$  in the soft-sphere case, but might correspond to a maximum for other potentials. The thermodynamic properties using a density-dependent breakpoint, again truncated after first-order terms, with  $\mu$  chosen to minimize the variation of  $A$  with  $\mu$ , are labeled Perturbation #2 in Fig. 4 and are tabulated in Table V. The variation of  $\mu$  with density on the isotherm  $\epsilon/kT = 1$  is shown in Fig. 6. At densities less than 0.3 the free energy minimum disappears. The theory at these low densities is insensitive to  $\mu$ , and the results for any choice in the range of values indicated in Fig. 6 lead to the same low-density  $PV/NkT$  within 0.01.

The perturbation theory is in quantitative agreement with the moderate-density machine results from about

TABLE VI. Comparison of solid-phase compressibility factors with cell-model and correlated-cell-model predictions. The static-lattice contribution to  $PV/NkT$  is  $24.264\rho^3\epsilon/kT$ .

$\rho(\epsilon/kT)^{1/4}$	$(PV/NkT)_\infty$	$(PV/NkT)_{\text{cell}}$	$(PV/NkT)_{\text{corr}}$
0.80	16.51	16.12	16.53
0.90	22.55	22.34	22.56
1.00	30.99	30.85	30.98
1.20	57.16	57.09	57.15

$\rho(\epsilon/kT)^{1/4} = 0.2$  to  $\rho(\epsilon/kT)^{1/4} = 0.4$ . At higher densities the pressure is too high, but never by more than 5%. The perturbation-theory melting transitions drawn in on Fig. 4 are a little misleading. In finding the transition locations for the perturbation theories it seemed reasonable to use also an approximate theory for the solid phase, namely, the cell model in which one particle moves in the field of its fixed neighbors. Because the free energy error in the perturbation theories at freezing is roughly the same as the free energy error in the cell model, about  $0.3NkT$ , the errors approximately cancel in determining the phase transition.

In describing the solid phase the lattice-dynamics approach can give an accurate calculation of the high-density entropy. At the same time, the anharmonic terms  $C_1$  and  $C_2$  found numerically show that the traditional lattice-dynamics perturbation theory, which estimates only  $C_1$  after considerable effort, is not accurate near the melting density. As an alternative route to  $C_1$  and  $C_2$ , we have explored two types of cell models (see Fig. 7). In either case the partition function is approximated by the  $N$ th power of a one-particle integral:

$$Z_{\text{cell}} \equiv \left[ \exp\left(-\frac{\Phi_0}{NkT}\right) \Lambda^{-3} \int_{\Delta} \exp\left(-\frac{\delta\phi}{kT}\right) d\mathbf{r} \right]^N, \quad (20)$$

where  $\delta\phi$  is the change in energy of the system as the particle moves from its lattice site to  $\mathbf{r}$ . The cell models are more easily calculated than the lattice-dynamics perturbation theories and do estimate anharmonic contributions to the pressure and the energy accurately.

In the simplest version of the cell model<sup>21</sup> the neighbors of the moving particle at  $\mathbf{r}$  are held fixed at their lattice sites. To simplify calculations the neighbors are often "smeared out" over a spherical surface, converting the integral in (20) to a one-dimensional integral. For soft spheres we have carried out both the exact non-smeared calculations and the smeared-out cell calculations. The results, given in Table VI, show that the cell-model value for  $C_1$  is about 30% too large and, with less sensitivity, that the cell-model  $C_2$  is nearly correct.

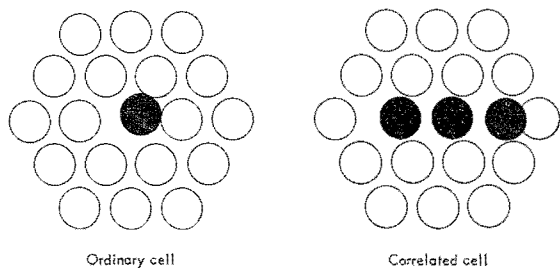


FIG. 7. Two kinds of cell models. The pressures from these models are compared with the soft-sphere Monte Carlo results in Table VI. In the ordinary cell model, one particle moves. In the correlated cell model three particles move cooperatively, with identical displacements from their lattice positions; the moving particles include the central particle and two neighbors—the two neighbors which would be respectively closest to and farthest from the central particle in the ordinary cell model.

Because the difference between the nonsmeared and smeared calculations was found not to exceed 0.02 in  $PV/NkT$  for the solid, only the smeared-cell results appear in the table.

Alder and Wainwright's movies of the two-dimensional hard-disk solid<sup>22</sup> show correlated motion of rows of particles in the solid, especially at densities near melting. A "correlated cell model" taking this motion into account<sup>23</sup> describes accurately the solid branch of the hard-disk isotherm, and produces a van der Waals loop in the vicinity of the hard-disk melting transition. For the soft spheres we have studied a correlated cell model which is nearly exact in its pressure predictions for the solid. In this correlated cell model the particle which would, in a perfect lattice, be closest to the moving particle moves cooperatively with it; a third particle, in line with these two, also moves (see Fig. 7). The model's success in predicting solid-phase pressures is outstanding. See Table VI for a comparison of the pressures from the Monte Carlo experiments and those from the cell model and the correlated cell model. Numerical estimates of the anharmonic coefficients from the correlated cell model are  $C_1=0.100$ ,  $C_2=-0.017$ , and  $C_3=0.0014$ . These coefficients describe the machine results just as well as our empirical choice,  $C_1=0.088$ ,  $C_2=-0.009$ . The specific heat for the correlated model is shown in Fig. 8 for comparison with the estimated specific heat from (16). The uncertainty in the Monte Carlo results is at least as great as the deviation between the two curves—the approximate anharmonic partition function including just  $C_1$  and  $C_2$  is not very reliable for predicting derivatives of the free energy of higher order than the first.

The maximum in the correlated-cell heat capacity is indicative of a high-order phase transition and is associated with the sliding motion of the atoms past each other. This interpretation is confirmed by inspecting numerical values of the integrand in (20) for the correlated model. At high densities the moving atom remains near its cell center, but as the density is decreased and melting approaches, there is a large

increase in the value of the integrand for the region between the correlated particles. This corresponds to the movement of atoms through the solid. Although the correlated model does not predict melting quantitatively, it does predict an order-disorder transition at about the density of the Monte Carlo melting transition. The heat-capacity maximum nearly coincides with the liquid's freezing density; it is unlikely that this coincidence will also occur for all other potentials.

Because the model does represent a breakup of the solid based on mechanical, as opposed to thermodynamic, grounds,<sup>24</sup> the density at which the breakup occurs does lie below the true thermodynamic melting density, in qualitative agreement with the Ross-Alder rule.<sup>25</sup> The specific heat maximum indicates that the model includes a mode of the kind needed to explain the large specific heats found in rare-gas crystals near melting. The specific heat increase occurs without the assumption of vacancies or other lattice defects. How well the correlated cell model heat capacity correlates with the melting curve for more realistic potentials is being investigated.<sup>26</sup>

Lindemann suggested that solids melt when the root-mean-squared displacement becomes a characteristic fraction of the nearest-neighbor spacing. With a few additional assumptions, this Lindemann melting rule takes the form

$$C_{\text{Lindemann}} = \theta (MV^{2/3}/T)_{\text{melt}}^{1/2}, \quad (21)$$

where  $\theta$  is  $h\nu_{\text{Debye}}/k$  and  $M$  is the gram atomic weight. This relation is exact along the soft-sphere melting line because the density dependences of  $\theta$ , proportional to  $\rho^{7/3}$  and  $(V^{2/3}/T)_{\text{melt}}^{1/2}$ , proportional to  $\rho^{-7/3}$ , cancel. The soft-sphere Lindemann constant, using the approximation  $(\nu_{\text{Debye}}/\nu_{\text{Einstein}})^2 \approx \frac{5}{3}$ , is 111, fairly close to the Lindemann constant for argon.

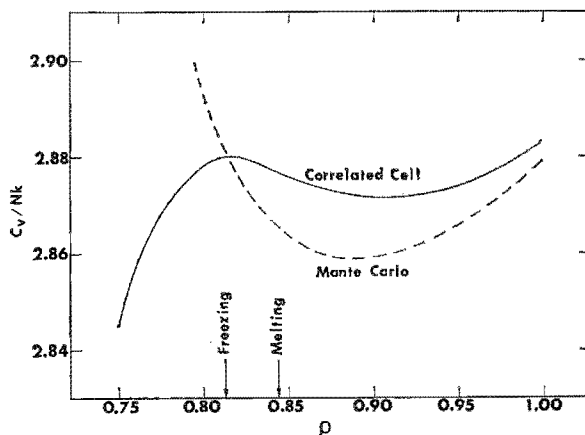


FIG. 8. The full curve shows the constant-volume specific heat from the correlated cell model along the isotherm  $\epsilon/kT=1$ . The dashed curve shows the estimate from soft-sphere Monte Carlo data. The uncertainty in the latter is comparable to the offset between the two curves. Note that the specific-heat maximum from the correlated cell model nearly coincides with the freezing density.

Ross has recently suggested that the Lindemann law be generalized to a theoretically more convenient form, by requiring that the nonideal part of the configurational partition function,<sup>36</sup>

$$Z^* \equiv \exp(-A^e/kT), \quad (22)$$

be constant along the melting line. As we see from the scaling in (4), this rule also holds for the soft-sphere potential.

Ashcroft and co-workers have a slightly different recipe for the melting line.<sup>37</sup> They suggested that the maximum in the Fourier transform of the pair distribution function be used to correlate the freezing densities of liquid metals. As another consequence of the soft-sphere scaling relation, the reduced distribution functions also depend upon the combination  $\rho^4\epsilon/kT$ . Thus the Fourier-transform maximum has a characteristic constant value in each phase along the melting line. Because the  $k$  characterizing the maximum scales as a reciprocal length, the position of the maximum varies as  $T^{1/2}$  along the melting line. Hansen and Verlet<sup>7,38</sup> have found that the Fourier-transform melting rule is *nearly* correct for the full Lennard-Jones potential; we expect they will soon report their detailed results.

#### ACKNOWLEDGMENTS

We would like to thank J.-P. Hansen, Laboratoire de Physique Théorique et Hautes Energies, 91-Orsay, France, for kindly keeping us informed of his progress on related Monte Carlo calculations he is carrying out. Hansen's independent estimate for the soft-sphere transition densities,  $0.813(kT/\epsilon)^{1/4}$  and  $0.844(kT/\epsilon)^{1/4}$ , agrees exactly with ours! We are grateful to Richard Grover, Albert Holt, and David Young, at Livermore, for stimulating discussions. Warren Cunningham assisted with most of the calculations on the 6600 and 7600 computers at Livermore, and Roger McLain expedited the drawing of the figures.

\* This work was carried out under the auspices of the U.S. Atomic Energy Commission.

† Summer employee at Livermore, 1969.

<sup>1</sup> F. H. Ree and W. G. Hoover, *J. Chem. Phys.* **40**, 939 (1964).

<sup>2</sup> B. J. Alder, W. G. Hoover, and D. Young, *J. Chem. Phys.* **49**, 3688 (1968). This paper contains occasional typographical errors.

<sup>3</sup> W. G. Hoover and F. H. Ree, *J. Chem. Phys.* **49**, 3609 (1968).

<sup>4</sup> Most of the computer results for hard spheres are summarized in a review by W. W. Wood, *Physics of Simple Liquids*, edited by H. N. V. Temperley, J. S. Rowlinson, and G. S. Rushbrooke (North Holland, Amsterdam, 1968), Chap. 5.

<sup>5</sup> M. Fixman, *J. Chem. Phys.* **51**, 3270 (1969).

<sup>6</sup> W. G. Rudd, Z. W. Salsburg, A. P. Yu, and F. H. Stillinger, *J. Chem. Phys.* **49**, 4857 (1968).

<sup>7</sup> J.-P. Hansen and L. Verlet, *Phys. Rev.* **184**, 151 (1969).

<sup>8</sup> L. Verlet, *Phys. Rev.* **159**, 98 (1967); **165**, 201 (1968).

<sup>9</sup> D. Levesque and L. Verlet, *Phys. Rev.* **182**, 307 (1969).

<sup>10</sup> In addition to Ref. 4, see I. R. McDonald and K. Singer, *J. Chem. Phys.* **47**, 4766 (1967).

<sup>11</sup> J. S. Rowlinson, *Mol. Phys.* **8**, 107 (1964); see also S. Kim, *Phys. Fluids* **12**, 2046 (1969).

<sup>12</sup> J. A. Barker and D. Henderson, *J. Chem. Phys.* **47**, 2856, 4714 (1967).

<sup>13</sup> R. W. Zwanzig, *J. Chem. Phys.* **22**, 1420 (1954).

<sup>14</sup> With perseverance, the necessary expressions can be extracted from the standard reference book by M. Born and K. Huang, *Dynamical Theory of Crystal Lattices* (Oxford U. P., London, 1954). See especially Secs. 24 and 29.

<sup>15</sup> J. O. Hirschfelder, C. F. Curtiss, and R. B. Bird, *Molecular Theory of Gases and Liquids* (Wiley, New York, 1954), pp. 41, 42.

<sup>16</sup> J. A. Barker, P. J. Leonard, and A. Pompe, *J. Chem. Phys.* **44**, 4206 (1966).

<sup>17</sup> R. O. Watts and D. Henderson, *J. Chem. Phys.* **50**, 1651 (1969).

<sup>18</sup> W. G. Hoover and B. J. Alder, *J. Chem. Phys.* **46**, 686 (1967).

<sup>19</sup> This result was derived with the help of Albert Holt. The mass associated with the center-of-mass coordinate is  $Nm$ , so that the momentum integration gives  $(2\pi Nm kT)^{3/2}$ .

<sup>20</sup> W. G. Hoover, *J. Chem. Phys.* **49**, 1981 (1968).

<sup>21</sup> G. Leibfried and W. Ludwig, *Solid State Phys.* **12**, 275 (1961).

<sup>22</sup> An analogous "multiple-occupancy" restriction has been used in Ref. 7 to help determine thermodynamic properties near the gas-liquid coexistence region of a Lennard-Jones fluid.

<sup>23</sup> D. R. Squire and W. G. Hoover, *J. Chem. Phys.* **50**, 701 (1969).

<sup>24</sup> C. H. Bennett and B. J. Alder, *Solid State Commun.* **6**, 785 (1968).

<sup>25</sup> This follows from the work of F. H. Stillinger, Z. W. Salsburg, and R. L. Kornegay, *J. Chem. Phys.* **43**, 932 (1965).

<sup>26</sup> Because at low enough density only pairs of particles can interact if the cells are spherical, it is possible to combine the integral (11) with Gaunt's dimer distribution [D. S. Gaunt, *Phys. Rev.* **179**, 174 (1969)] to calculate the exact low-density hard-sphere single-occupancy isotherm to order  $\rho^{15}$  in  $PV/NkT$ . Because the radius of convergence of this long series is probably small, we have not carried out a detailed investigation.

<sup>27</sup> A system artificially restricted to be either pure fluid or pure solid would exhibit a vertical jump on a pressure versus volume plot. The jump would occur at the density for which the Helmholtz free energies of the (metastable) pure phases are equal. The "equal-area" tie line cuts the vertical portion at a pressure for which the Gibbs free energies of the pure phases are equal. The two approximately triangular regions produced by the cut have equal areas. A similar use of the equal-area rule, applied to an isotherm for a system restricted to pure-phase states, can be found in R. W. Zwanzig, *J. Chem. Phys.* **39**, 1714 (1963).

<sup>28</sup> M. Ross and B. J. Alder, *Phys. Rev. Letters* **16**, 1077 (1966).

<sup>29</sup> See the comprehensive Table 5 in Ref. 4.

<sup>30</sup> R. Grover, *Bull. Am. Phys. Soc.* **13**, 1647 (1968).

<sup>31</sup> See John A. Barker, *Lattice Theories of the Liquid State* (Pergamon, Oxford, 1963), and pp. 286-304 of Ref. 15 for a description of cell-theory ideas.

<sup>32</sup> These movies were made at Livermore about five years ago and have not been distributed outside the laboratory.

<sup>33</sup> The correlated cell model described by B. J. Alder, W. G. Hoover, and T. E. Wainwright, *Phys. Rev. Letters* **11**, 241 (1963), was based on an earlier calculation by D. R. Squire and Z. W. Salsburg, *J. Chem. Phys.* **35**, 486 (1961).

<sup>34</sup> J. Frenkel, *Kinetic Theory of Liquids* (Dover, New York, 1955), Chap. III, Sec. 6.

<sup>35</sup> M. Ross is investigating the Lennard-Jones potential melting line with the aid of the correlated cell model.

<sup>36</sup> M. Ross, *Phys. Rev.* **184**, 233 (1969).

<sup>37</sup> N. W. Ashcroft and J. Lekner, *Phys. Rev.* **145**, 83 (1966); N. W. Ashcroft and D. C. Langreth, *Phys. Rev.* **159**, 500 (1967).

<sup>38</sup> Dr. Hansen informs us that he is testing the structure-factor criterion at temperatures higher than those treated in Ref. 7.